Cross sections for H^+ and H atoms colliding with Li in the low-keV-energy region

R. Cabrera-Trujillo
Instituto de Ciencias Físicas, Universidad Nacional Autónoma de México, Apartado Postal 48-3, Cuernavaca, Morelos, 62210, Mexico

John R. Sabin, E. Deumens, and Y. Öhrn
Quantum Theory Project, Departments of Chemistry and Physics, University of Florida, P.O. Box 118435, Gainesville, Florida, 32611-8435, USA

(Received 23 April 2008; published 22 July 2008)

State-to-state, summed charge transfer and stopping cross sections in collisions of protons and neutral hydrogen atoms with lithium atoms have been studied at collision energies ranging from 10 to 25 keV. Cross sections were calculated using electron-nuclear dynamics (END), which is a nonadiabatic, time-dependent, direct approach for the study of ion-atom-molecule interaction processes. Our results show good agreement when compared to available theoretical and experimental data. We find that the charge transfer cross section for protons shows a bump and a maximum as a function of the projectile energy, both of them as a result of the large probability for capture into the projectile $2p$ orbital. The bump corresponds to a projectile energy of approximately $E_p \sim 0.7$ keV, and results from the electron capture probability in the low impact parameter region of approximately $b \sim 2.0$ a.u. The maximum occurs at $E_p \sim 5$ keV as a result of the larger capture probability in the intermediate impact parameter region near $b \sim 8$ a.u. A similar behavior is found for the electron loss cross section for hydrogen projectiles. We find that the beam charge fraction, for all the energies considered, is nearly neutral. We also find that the largest contribution to the stopping cross section is for impact parameters around $b \sim 5$ a.u. Finally, we report the total, electronic, and nuclear stopping cross sections to be within a factor of 2 of the reported values in the SRIM 06 code (SRIM stands for stopping and range of ions in matter) and other available experimental data. The largest discrepancy is due to the charge transfer process as well as to a transient LiH^+ molecular ion formed in the low projectile energy region.

DOI: 10.1103/PhysRevA.78.012707 PACS number(s): 34.70.+e, 34.50.Bw

I. INTRODUCTION

Understanding of the details of collisions of swift ions with atoms and molecules is essential for explanation and prediction of many processes in physics, ranging from radiobiology to atmospheric chemistry. Such collisions may result in charge transfer and energy loss processes for which cross sections must be calculated and understood in order to fully explain the process under investigation. Recently, a proposal has been suggested for the International Thermonuclear Experimental Reactor (ITER) project in which MeV energy negatively charged deuterium ions in lithium gas charge exchange cells might produce high energy neutral lithium atoms which could then be used for heating the ITER fusion plasma. In such a charge exchange environment, a secondary reaction involving neutral or singly positively charged ions with lithium could be expected. In this circumstance, cross sections for collision with lithium would be useful [1]. We model this situation with protons and hydrogen atoms.

In the case of protons colliding with lithium atoms, the electron capture (neutralization) occurs mainly into the $n=2$ state of hydrogen and is nearly resonant. There have been already some theoretical studies of this collision system. The molecular-orbital calculations of Allan *et al.* [2] are in agreement with the modified atomic orbital results of Fritsch and Lin [3]. However, they differ somewhat from the results of Sato and Kimura [4], and with the atomic orbital results of Ermolaev [5]. All of these studies are in the keV projectile energy region based on potential energy curves (PEC) or coupled-channel methods. Recently, the theoretical results of Errea *et al.* [6] partially address the electron capture cross section for collision energies as low as 10 eV for the case of protons colliding with lithium atoms.

Conventional methods that proceed via predetermined PEC are difficult to implement when numerous such curves and corresponding stationary electronic states are involved. So-called direct methods that treat the reaction dynamics in terms of the instantaneous Coulombic forces between participating electrons and atomic nuclei exist, but when the requirement is added that nonadiabatic processes must also be included, then there are, indeed, very few approaches available. One such method is electron nuclear dynamics (END) [7]. This time-dependent approach has been successfully applied to a number of ion-atom collisions [8,9]. The present study of hydrogen and proton beams on lithium atoms is an attempt to understand some of the details of such processes using a system which is simple enough so that our theoretical approach is predictive.

In this paper, we address the total as well as the state-to-state electron capture cross section for protons colliding with atomic Li for projectile energies from 10 eV up to 25 keV by means of the END method. Furthermore, we consider neutral hydrogen projectiles and study the beam charge fraction, projectile energy loss, and stopping cross section. The paper is presented in the following structure: In Sec. II, we provide an overview of the theoretical basis and computational implementation of the method. In Sec. III, we present our results starting with the electron capture probability in Sec. III A, followed by the summed electron transfer cross section in Sec. III B, and the state-to-state electron capture cross section in Sec. III C. In Sec. III D we present the electron loss cross section. In Sec. III E the beam charge fraction

results are provided. In Sec. III F the projectile kinetic energy loss is presented. The results of the previous sections are combined in Sec. III G to obtain the stopping cross section. Finally, in Sec. IV we present our conclusions.

II. THEORETICAL AND COMPUTATIONAL APPROACH

A. END method

END [7] is the theoretical approach used here to study proton collisions with lithium atoms at keV energies. This is an *ab initio*, explicitly time-dependent theory that accounts for nonadiabatic effects. The simplest approximation, which is used in the present work, employs a single, so-called Thouless [10], determinant description of the electrons, where the spin orbitals are complex linear combinations of atomic Gaussian functions centered on the average nuclear positions, and commonly endowed with electron translation factors. Nuclei are treated as Gaussian wave packets in the narrow width limit, which is equivalent to the nuclei moving as classical particles. The dynamics takes place in a Cartesian laboratory coordinate frame, thus translational and rotational degrees of freedom are included.

Wave function parameters, such as average nuclear position coordinates and momenta, and complex molecular orbital coefficients carry the time-dependence and serve as the dynamical variables of the problem. Using the common symbols ζ and ζ^* for all dynamical variables, namely the time-dependent parameters in the evolving state vector $|\zeta\rangle$, the END equations of motion take the form

$$\begin{pmatrix} 0 & -iC^* \\ iC & 0 \end{pmatrix} \begin{pmatrix} \dot{\zeta} \\ \dot{\zeta}^* \end{pmatrix} = \begin{pmatrix} \partial E/\partial \zeta \\ \partial E/\partial \zeta^* \end{pmatrix}, \tag{1}$$

where the total energy is the average of the total molecular Hamiltonian, $E=\langle\zeta|H|\zeta\rangle/\langle\zeta|\zeta\rangle$ and the dot superscript denotes differentiation with respect to the time parameter, t. The detailed forms of the coupling terms C and C^* of the so-called dynamical metric can be found in Ref. [7].

Integration of these coupled first-order differential equations offers some challenges because of the usually very different time scales of electron and nuclear dynamics. The code uses a variety of quadratures most of which can be found in the standard literature [11]. The code that implements the theory is called appropriately *ENDyne* [12]. Thus at the end of the time evolution, we obtain the electronic wave function, and the nuclear positions and momenta. From these quantities we obtain the properties reported in this work.

B. Calculation details

The target is placed at the origin of the Cartesian laboratory coordinate system and the projectile is placed at a distance sufficiently large so that the interaction with the target is minimal, and with a momentum commensurate with the collision energy. In this particular case, we place the projectile at a distance of 100 a.u. beyond the target due to the very diffuse $2s$ orbital of Li. The dynamics is stopped when the projectile has passed 200 a.u. from the target or until there is no further change in the charge transfer probability due to interactions of the projectile and target electronic cloud. The initial conditions include the determination of a proper electronic state of the target-projectile system.

TABLE I. Basis set orbital exponents for Li and H atoms.

	Li		H		
i	α_s	α_p	α_s	α_p	α_d
1	16.1195748	0.6362897	33.870000	1.407000	1.057000
2	2.9362007	0.1478601	5.095000	0.388000	0.247000
3	0.7946505	0.0480887	1.159000	0.102000	0.069937
4	0.6362897	0.0014936	0.325800	0.029064	0.019803
5	0.1478601	0.0004978	0.102700	0.008281	
6	0.0480887		0.025260	0.002360	
7	0.0014936		0.005984		
8	0.0004978		0.001417		

A proper choice of basis set is crucial in this method. We use Gaussian basis sets of the form

$$\varphi_i(\mathbf{r}) = \sum_j d_{ij}(x-R_x)^n(y-R_y)^m(z-R_z)^l e^{-\alpha_j(\mathbf{r}-\mathbf{R}_i)^2} \tag{2}$$

centered on the average nuclear positions $\mathbf{R}_i$ with exponents α_j and coefficients d_{ij}. From these we form linear combinations of atomic orbitals which become the molecular orbitals of the system. For the Li target we obtain a self-consistent field ground state for the $1s^22s$ configuration by means of a $[6s3p/2s1p]$ basis set from Pople [13], augmented by two s and two p even-tempered diffuse orbitals to allow for low lying excited states of the target. For the projectile we used a $[6s3p2d/4s3p2d]$ basis set from Dunning [14], augmented by two s and two p even-tempered diffuse orbitals to reproduce the low hydrogenic excited states. The exponents used in our calculations for the basis set are given in Table I. The orbital energies obtained by this basis set for the case of hydrogen are $E(1s)=-0.499\,339\,8$, $E(2s)=-0.123\,928\,6$, $E(2p)=-0.123\,876\,8$, $E(3s)=-0.0557\,926$, $E(3p)=-0.055\,334\,8$, and $E(3d)=-0.052\,081\,5$ in Hartree a.u.

A number of END trajectories are run with different impact parameters ranging from 0.0 up to 40 a.u. We consider three ranges of impact parameter: (1) the close interaction region that goes from 0.0 up to 10.0 a.u. in steps of 0.1 a.u.; (2) the intermediate region covers the range from 10 to 20 a.u. in steps of 0.5 a.u.; and (3) the long range interaction region covers the impact parameters from 20 to 40 a.u. in steps of 1.0 a.u. This yields trajectories for a total of 141 impact parameters per projectile energy. The projectile energies considered are 10, 18, 30, 50, 90, 150, 300, 500, 700, 1000, 1500, 2000, 3000, 5000, 7000, 10 000, 16 000, and 25 000 eV, respectively. Thus, in total, over 7600 trajectories have been run. The probability of electron capture and energy loss are thus calculated from these trajectories to obtain charge transfer and stopping cross sections.

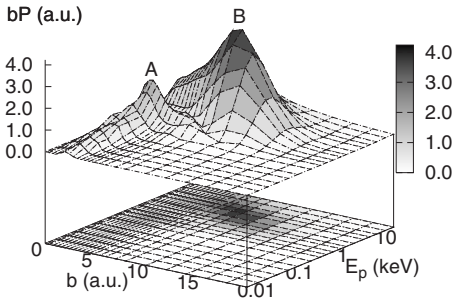

FIG. 1. Capture probability into the $2p$ hydrogen orbital for protons colliding with Li as a function of the projectile impact parameter and energy. Note the two maxima at $A=(b\sim 2$ a.u., $E_p\sim 0.7$ keV) and $B=(b\sim 8$ a.u., $E_p\sim 5$ keV).

III. RESULTS

A. Electron capture probability

The electron capture probability is obtained by projecting the final evolved electronic wave function on a particular electronic state of the projectile, expressed in terms of the projectile basis set. The probability for finding the electron in that final state Ψ_f is thus given by $P_f(b)=|\langle\Psi_f|\Psi_j\rangle|^2$ where Ψ_j is the electronic state wave function at the end of the dynamics as a result of being initially in the j state. Ψ_f is a particular stationary electronic state on the projectile we are interested in, e.g., the $1s$ state of hydrogen.

In Fig. 1, we show the capture probability for finding the electron captured into the $2p$ orbital of the hydrogen projectile as a function of the projectile impact parameter and collision energy. A bump at $A=(b\sim 2$ a.u.,$E_p\sim 0.7$ keV) and maximum at $B=(b\sim 8$ a.u.,$E_p\sim 5$ keV) can be observed. The electron capture probability decreases for lower projectile energies in the small impact parameter region. Furthermore, it presents a ridge around $b\sim 2$ a.u. from the low projectile energy region that starts at peak A. This ridge accounts for the electron capture in the low projectile region.

B. Electron capture cross section

The electron capture cross section into a final state f of the projectile is calculated from the electron capture probability as

$$\sigma^f(E_p)=2\pi\int_0^\infty bP_f(b,E_p)db. \tag{3}$$

In Fig. 2, we show the total (summed) electron capture cross section, σ_{10}, for protons colliding with atomic Li as a function of the projectile energy. Here, σ_{if} is the total cross section where i refers to the initial projectile charge state, and f to the final projectile charge state. We compare our results with the experimental data of Varghese [15] and DuBois [16], as well as with the theoretical results of Errea [6] and Fritsch and Lin [3]. The quantum mechanical results of Errea and our results are very close in the low energy region and start to separate in the intermediate energy region, as shown in Fig. 3, which depicts more details near the maximum of the electron capture cross section.

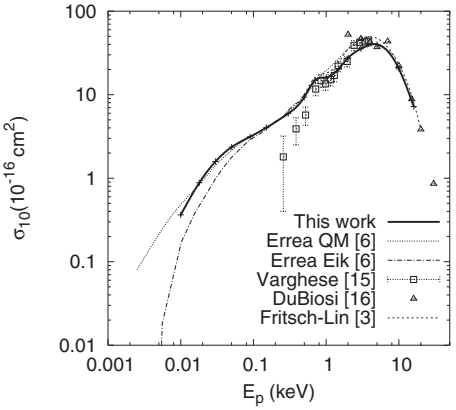

FIG. 2. Total charge transfer cross section for protons colliding with Li as a function of the projectile energy. Solid thick line: this work; dotted line: Errea's quantum mechanics calculation [6]; dashed-dotted line: Errea's eikonal approximation [6]; long-dashed line: Fritsch and Lin [3] experimental data: □, Varghese [15]; and ◇, DuBois [16].

We note that there is a bump and a maximum in the electron capture cross section as a function of the projectile energy. From Fig. 1, it is evident that these features are related to the peaks (A) and (B) in the electron capture probability. Furthermore, the bump at A coincides with the experimental counterpart of Varghese [15]. At projectile energies between 2 and 3 keV, our results are below the other theoretical results, but follow the experimental trend of Varghese [15].

C. State to state electron capture cross section

In Fig. 4, we show the state-to-state capture cross section into the $1s$, $2s$, $2p$, $3s$, and $3p$ hydrogen orbitals for protons colliding with Li atoms and compare with the experimental results of Aumayr *et al.* [17]. For projectile energies larger than 15 eV the dominant electron capture channel is into the hydrogen $2p$ orbital. For projectile energies lower than $E_p<15$ eV, it seems that capture into the $2s$ orbital dominates, thus showing a crossing between the $2p$ and $2s$ contributions.

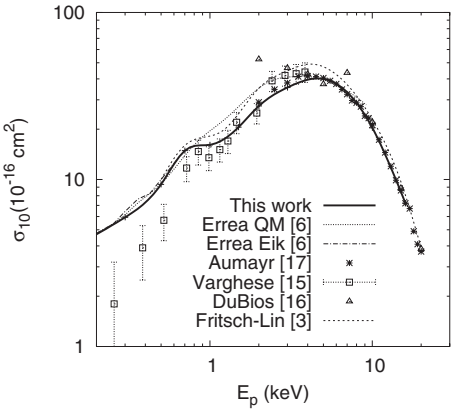

FIG. 3. Charge transfer cross section for protons colliding with Li as a function of the projectile energy. Labels as in Fig. 1, with the addition of Aumayr *et al.* experimental points (*) [17] at high projectile energies.

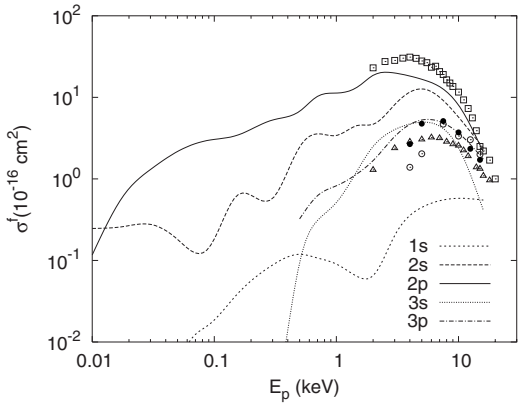

FIG. 4. State-to-state charge transfer cross section into the final state f of the projectile, σ^f, for protons colliding with Li, as a function of the projectile energy. This work: short-dashed line: $1s$ electron capture cross section; long-dashed line: $2s$ electron capture cross section; solid line: capture into the hydrogen $2p$ orbital; dotted line: capture into the $3s$; long dashed-dotted line: capture into the $3p$. Experimental data is from Aumayr *et al.* [17]: □, $2p$; ●, $3p$ Hα line; ○, $3s$; and △, $3d$.

A detailed study in the lower projectile energy region is under way to help with understanding of this crossing.

Figure 5 shows a detailed view of Fig. 4 for the projectile energy region between 1 and 25 keV where we have summed the contributions of the l states for a given quantum number n of the projectile. First, we note that $n=1$ is the lowest contribution to the capture cross section of the three lowest n states, followed by $n=3$. The dominant channel at the peak of the total cross section is $n=2$. In the same figure, we compare with the theoretical data of Fritsch and Lin [3] with reasonably good agreement for the three states.

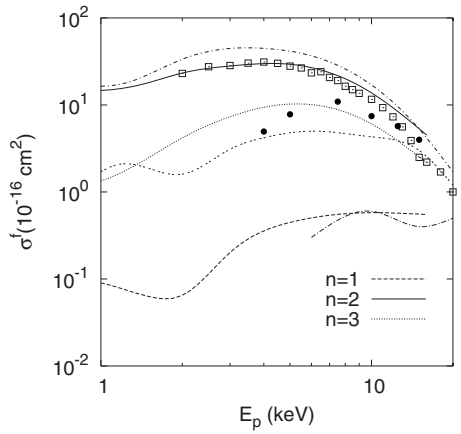

FIG. 5. State-to-state charge transfer cross section, σ^f, summed over the l states of a given quantum number n of the projectile for protons colliding with Li as a function of the projectile energy. This work: solid line ($n=2$); dotted line ($n=3$); and dashed line ($n=1$). The theoretical results of Fritsch and Lin [3] are shown for comparison: Dotted-long dashed line ($n=1$); dotted-short dashed line ($n=2$); and dashed-dashed line ($n=3$). Experimental data from Aumayr *et al.* [17]: □, $n=2$; and ●, $n=3$.

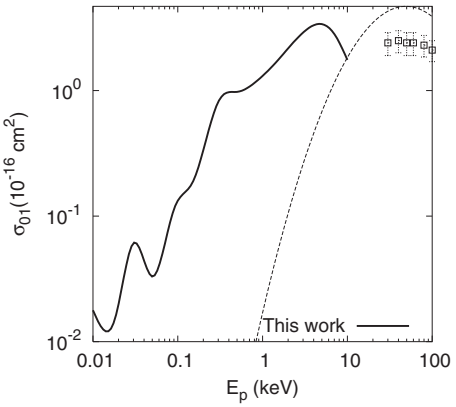

FIG. 6. Electron loss cross section, σ_{01}, for neutral hydrogen projectiles colliding with atomic Li as a function of the projectile energy. Solid thick line: this work. The experimental points are from Anderson *et al.* [18] and the dashed line is the scaling law results of Santos and DuBois [19].

D. Electron loss cross section

For the case of neutral hydrogen colliding with atomic lithium, we show in Fig. 6 the electron loss cross section, σ_{01}, as a function of the projectile energy and compare with the experimental data of Anderson *et al.* [18] and the scaling (fitting) results of Santos and DuBois [19]. The peak of our theoretical result is shifted to lower energy when compared to the scaling law of Santos and DuBois although the slope and trend is similar. The maximum in the calculated curve is of the same order of magnitude as the experimental points of Anderson. A possible reason for the discrepancy is that the ionization channel is not open in our calculations.

A noticeable characteristic of the electron loss cross section is that it shows a similar bump as in the electron capture cross section, but instead of being placed around 0.7 keV, it is around 0.3 keV. This bump is not reproduced by the scaling laws of Santos and DuBois.

E. Beam charge fraction

From the electron capture and loss cross section, one can determine the fraction of protons and neutral hydrogen in the beam by assuming that the number of particles is conserved in the beam. Thus the fraction of protons is proportional to the number of neutral hydrogen atoms stripped of the electron [20], i.e.,

$$f(H^+) = \frac{\sigma_{01}}{\sigma_{10} + \sigma_{01}}. \tag{4}$$

The fraction of neutral hydrogen is proportional to the number of neutralized protons, that is

$$f(H^0) = \frac{\sigma_{10}}{\sigma_{10} + \sigma_{01}}. \tag{5}$$

These results are obtained under the assumption that the fraction of hydrogen anions can be neglected [20].

In Fig. 7, we show the beam charge fraction as a result of combining the data of Figs. 2 and 6 into Eqs. (4) and (5). The

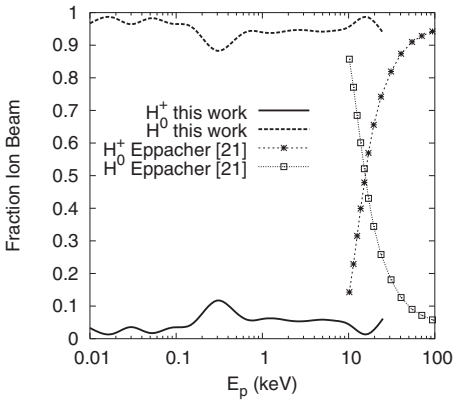

FIG. 7. Beam charge fraction as obtained from considering the electron capture and loss cross section for protons and hydrogen atoms colliding with atomic Li as a function of the projectile energy. The H^- fraction has been neglected. The experiments are the results of Eppacher *et al.* [21].

result shows that, for almost all the projectile energies considered here, the beam charge is nearly neutralized. This can be seen as a consequence of the large electron capture cross section of protons colliding with lithium, or as a result of the low ionization potential of lithium. In the same figure, we compare with the results reported by Eppacher [21] which show that at higher projectile energies than those considered here, i.e., $E_p > 25$ keV, the stripping of electrons from the projectile starts to dominate. We also notice that the bump in σ_{01} around 0.3 keV shown in Fig. 6 is reflected in the beam charge fraction. Due to the lack of an open ionization channel in these calculations, we have not extended our study to higher projectile energies, particularly for the neutral hydrogen.

F. Kinetic energy loss

From the final projectile momenta, we obtain the projectile kinetic energy. In Fig. 8, we show the projectile kinetic energy loss times the impact parameter as a function of the impact parameter and projectile initial energy. The largest kinetic energy loss occurs for impact parameters around $b \sim 5$ a.u. and keeps increasing as a function of the projectile energy considered in this work. Also, we notice that there is

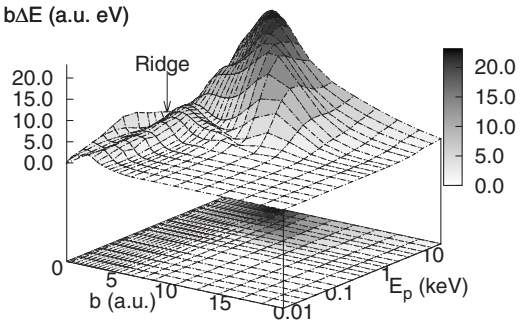

FIG. 8. Projectile kinetic energy loss as a function of the initial projectile energy and impact parameter for protons colliding with atomic lithium.

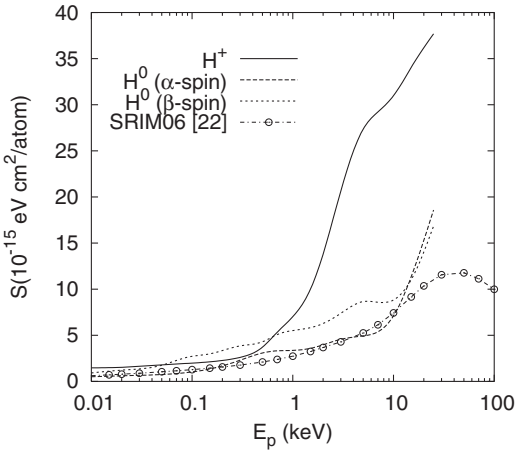

FIG. 9. Total stopping cross section for protons and hydrogen projectiles colliding with atomic lithium as a function of the projectile energy. The results for neutral hydrogen are shown for the two cases where the projectile electron has α vs β spin. For comparison, we also show the results from the SRIM 06 program [22].

a ridge for $b \sim 2$ a.u. for the low projectile energy region similar to the ridge that appears in the electron capture cross section, thus correlating the energy loss with the electron capture.

G. Stopping power and stopping cross section

The stopping power, which is the projectile energy loss per unit path per target atom, is obtained from the kinetic energy loss as

$$S(E_p) = -\frac{1}{n}\frac{dE}{dx} = \int b\Delta E(E_p,b)dbd\varphi. \tag{6}$$

Total stopping cross section. In Fig. 9, we show the total stopping cross section, $S(E_p)$, for protons and neutral hydrogen projectiles as they penetrate a lithium gas, as a function of the initial projectile energy. Due to the large electron capture probability for protons when colliding with a lithium atom, the stopping cross section is also larger than that of the neutral projectile for large projectile energies. We also show, in the same figure, the energy loss for the case of neutral projectiles when the projectile has an α-spin electron versus a β-spin electron under the assumption that the $2s$ electron on the target Li is always an α-spin electron. These results show that the α-spin projectile electron has a lower contribution, due to the Pauli exclusion principle, than does the projectile β-spin electron which will pair with the one on the target, and more effectively slowing down the projectile.

When we make use of the beam charge fraction, the averaged stopping cross section is obtained by

$$S_a(E_p) = f(H^+)S(H^+) + f(H^0)S(H^0). \tag{7}$$

The results are shown in Fig. 10 and are compared with the results of Eppacher [21] and the numerical data obtained by means of stopping and range of ions in matter (SRIM) 06 [22]. We note that for energies below 10 keV, our results are within a factor of 2 when compared to the results obtained by

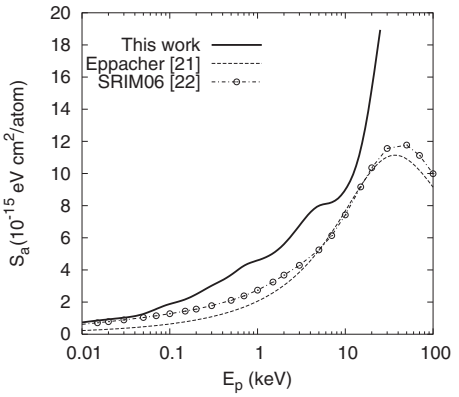

FIG. 10. Averaged total stopping cross section, S_a, for a hydrogen beam colliding with atomic lithium as a function of the beam energy. The dashed line corresponds to the results of Eppacher [21] and the symbol-line data are those obtained from SRIM 06 [22].

SRIM 06. Our averaged present results have two small bumps, one at $E_p \sim 5$ keV and another around $E_p \sim 0.7$ keV. Both of them seem to be correlated with the peak of the electron capture and loss cross sections discussed previously.

Nuclear stopping cross section. By calculating the kinetic energy gained by the target during the collision, we obtain the nuclear stopping cross section. In Fig. 11, we show the results for the nuclear stopping cross section for protons and neutral hydrogen projectiles as they collide with atomic lithium. In the same figure we compare with the results from SRIM 06. The proton stopping cross section shows a larger contribution in the lower projectile energy region than that shown by the neutral hydrogen projectiles. The reason is that at those energies there is a transient LiH^+ molecule formed that slows down the proton more than it does the neutral hydrogen projectile. However, due to the dominance of neutral hydrogen in the beam, the averaged nuclear cross section

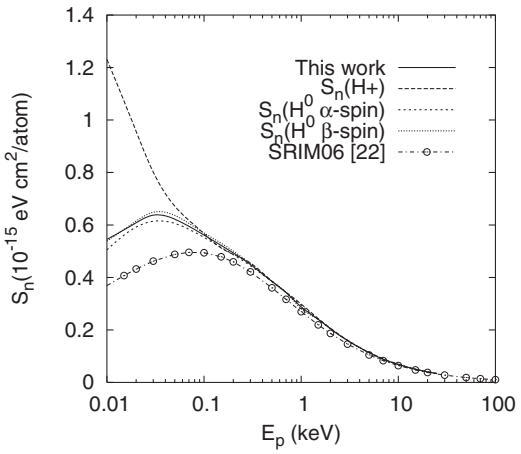

FIG. 11. Nuclear stopping cross section for protons and neutral hydrogen projectiles colliding with atomic lithium. Solid line: averaged nuclear stopping cross section; dashed line: nuclear stopping cross section for protons; short-dashed line: nuclear stopping cross section for neutral hydrogen colliding with an α-spin electron; dotted line: nuclear stopping cross section for neutral hydrogen colliding with a β-spin electron. The data from SRIM 06 are for the nuclear contribution to the stopping cross section [22].

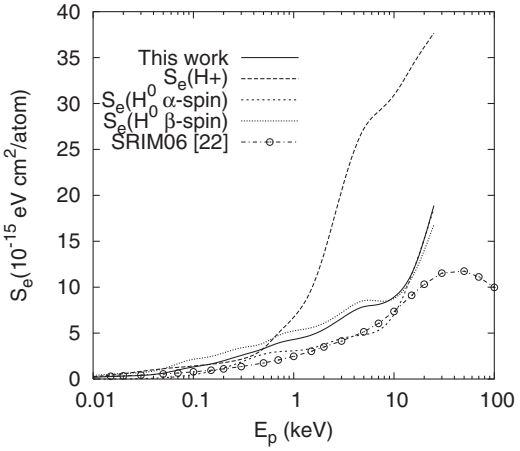

FIG. 12. Electronic stopping cross section for protons and neutral hydrogen projectiles colliding with atomic Li. The results of SRIM 06 [22] are also shown.

is very similar to that reported by SRIM 06 (solid line) for projectile energies $E_p > 0.5$ keV. Our results show a larger maximum around $E_p \sim 30$ eV than does SRIM 06, which shows the maximum around $E_p \sim 100$ eV, probably due to the screening and electron transfer and loss processes not properly taken into account in SRIM 06.

Electronic stopping cross section. Subtracting the nuclear stopping cross section from the total stopping cross section leaves us with the electronic stopping cross section, which includes the energy loss due to excitations and electron capture and loss taking place during the collision. We show in Fig. 12 our results for the electronic stopping cross section for protons and neutral hydrogen projectiles colliding with atomic lithium as a function of the projectile energy and compare them with the data of SRIM 06.

In the higher energy region, we note that the largest contribution is from the proton projectile where the largest electron capture cross section occurs. However, due to the dominance of the neutral hydrogen projectile in the beam, its contribution is not reflected in the averaged electronic stopping cross section. Again, we notice that when we compare with the data from SRIM 06, our averaged electronic stopping cross section is within a factor of 2 larger. Furthermore, our results show a bump around $E_p \sim 5$ keV consistent with the correlation of electron capture and loss in the cross section results as shown in Figs. 2 and 6.

IV. CONCLUSIONS

In this work we have presented the total, state-to-state electron capture and loss cross section, beam charge fraction, projectile kinetic energy loss, and stopping cross sections for protons and neutral hydrogen atoms colliding with atomic Li by means of a nonadiabatic, fully coupled electron-nuclei dynamics. We show that the main electron capture channel for protons is into the $2p$ state of hydrogen, which exhibits a bump and a maximum: the bump at around $E_p \sim 0.7$ keV and the maximum at $E_p \sim 5$ keV. The lower energy maximum

corresponds to a small impact parameter collision region while the second and larger one corresponds to large impact parameter regions. We also report the beam charge fraction, finding that the neutral beam fraction is dominant for the energies considered in this work. Finally, we also report our results for the total, electronic, and nuclear stopping cross section. Our results show good agreement with existing models and a good accord with experimental data. We also have considered the case of spin effects in the stopping cross section for neutral hydrogen atoms with spin up and down (α and β spin) showing different contributions. We hope this work will motivate more experimental and theoretical studies for hydrogen beam colliding on atomic Li in the gas phase.

ACKNOWLEDGMENTS

This work was completed with support of NSF Grant No. 00057476 to NYÖ. We acknowledge the support of the University of Florida's High Performance Computing center for the facilities provided for the development of this work. We would like to acknowledge the wonderful discussions with Professor N. Stolterfoht and Professor S. A. Cruz.

[1] L. R. Grisham, Phys. Plasmas **14**, 102509 (2007).
[2] R. J. Allan, A. S. Dickinson, and R. McCarroll, J. Phys. B **16**, 467 (1983).
[3] W. Fritsch and C. D. Lin, J. Phys. B **16**, 1595 (1983).
[4] H. Sato and M. Kimura, Phys. Lett. **96A**, 286 (1983).
[5] A. M. Ermolaev, in *Abstracts of Contributed Papers, Thirteenth International Conference on the Physics of Electronic and Atomic Collisions, Berlin, 1983*, edited by J. Eichler, W. Fritsch, I. V. Hartel, N. Stolterfoht, and U. Wille (ICPEAC, Berlin, 1983), p. 514.
[6] L. F. Errea, F. Guzmán, L. Méndez, B. Pons, and A. Riera, Phys. Rev. A **77**, 012706 (2008).
[7] E. Deumens, A. Diz, R. Longo, and Y. Öhrn, Rev. Mod. Phys. **66**, 917 (1994).
[8] R. Cabrera-Trujillo, J. R. Sabin, Y. Öhrn, and E. Deumens, Phys. Rev. A **61**, 032719 (2000).
[9] B. J. Killian, R. Cabrera-Trujillo, E. Deumens, and Y. Öhrn, J. Phys. B **37**, 4733 (2004).
[10] D. J. Thouless, Nucl. Phys. **21**, 225 (1960).
[11] W. H. Press, S. A. Teukolsky, W. T. Vetterling, and B. P. Flannery, *Numerical Recipes*, 2nd ed. (Cambridge University Press, New York, 1992).
[12] E. Deumens, T. Helgaker, A. Diz, H. Taylor, J. Oreiro, B. Mogensen, J. A. Morales, M. C. Neto, R. Cabrera-Trujillo, and D. Jacquemin, *ENDyne version 5 Software for Electron Nuclear Dynamics*, Quantum Theory Project (University of Florida, Gainesville, FL, 2002), http://www.qtp.ufl.edu/endyne.html.
[13] W. Hehre, R. F. Stewart, and J. A. Pople, J. Chem. Phys. **51**, 2657 (1969).
[14] T. H. Dunning, J. Chem. Phys. **90**, 1007 (1989).
[15] S. L. Varghese, W. Waggoner, and C. L. Cocke, Phys. Rev. A **29**, 2453 (1984).
[16] R. D. DuBois and L. H. Toburen, Phys. Rev. A **31**, 3603 (1985).
[17] F. Aumayr, M. Fehringer, and H. Winter, J. Phys. B **17**, 4201 (1984).
[18] C. J. Anderson, R. J. Girnius, A. M. Howald, and L. W. Anderson, Phys. Rev. A **22**, 822 (1980).
[19] A. C. F. Santos and R. D. DuBois, Phys. Rev. A **69**, 042709 (2004).
[20] A. Dalgarno and G. W. Griffing, Proc. R. Soc. London, Ser. A **232**, 423 (1955).
[21] C. Eppacher, R. D.-M. No, S. Semrad, and A. Arnau, Nucl. Instrum. Methods Phys. Res. B **96**, 639 (1995).
[22] J. F. Ziegler, J. P. Biersack, and U. Littmark, *The Stopping and Range of Ions in Solids* (Pergamon Press, New York, 2006).